

We are IntechOpen, the world's leading publisher of Open Access books Built by scientists, for scientists

5,800

Open access books available

142,000

International authors and editors

180M

Downloads

Our authors are among the

154

Countries delivered to

TOP 1%

most cited scientists

12.2%

Contributors from top 500 universities



WEB OF SCIENCE™

Selection of our books indexed in the Book Citation Index
in Web of Science™ Core Collection (BKCI)

Interested in publishing with us?
Contact book.department@intechopen.com

Numbers displayed above are based on latest data collected.
For more information visit www.intechopen.com



Binary Semiconductors Thin Films Characterization for Solar Cells Applications

Kenza Kamli and Zakaria Hadeif

Abstract

The increasing development of technologies based on the thin films, imposed a high quality of these films. The crucial importance for all applications of thin films is related to the stability of their physical and morphological properties. Therefore, to optimize the performances of the thin films it is recommended to study carefully all their parameters in order to enhance the elaborated films. With this intention, various characterizations methods were developed and carried out to study the different qualities of thin films. In this chapter, we take an interest to the study of the characteristics of some binary semiconductors thin films elaborated by ultrasonic spray pyrolysis, and which are destined for solar cells applications. Several used characterizations techniques to the determination of the thin films properties will be given; namely: X-rays diffraction (XRD), Scanning Electron Microscopy (SEM), EDS (Energy Dispersive Spectroscopy), Hall effect and spectrophotometry will be discussed in detail.

Keywords: Thin films, ultrasonic spray, X-rays diffraction, SEM, EDS, spectrophotometry, Hall effect, Binary semiconductors

1. Introduction

The materials have different properties, which are described by their structure, morphology and chemical composition. The determination of these properties and the study of the different characteristics of the given materials in order to their development is very necessary to achieve the requirements of the new technologies. Therefore, materials characterization is a fundamental process in the field of materials science.

While many characterization techniques have been practiced for centuries, such as basic optical microscopy, but new techniques and methodologies are constantly emerging. Detection ranges of the wide variety of instrumental analytical techniques can be summarized versus the probe sizes/resolution as shown in **Figure 1**.

This chapter is devoted to describe certain important characterization techniques used in general to study and develop the different characteristics of certain binary semiconductors thin films, which are used in solar cells, to get layers with high performances.

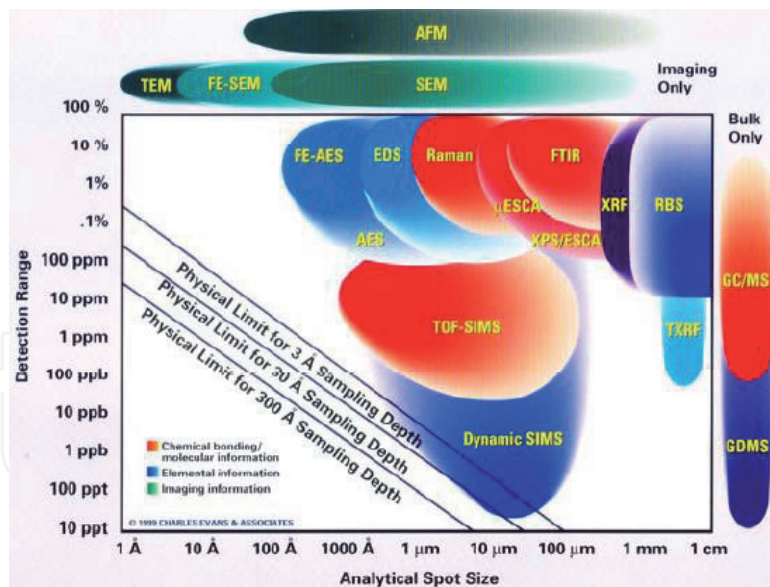


Figure 1.
Schematic of detection ranges versus probe sizes/resolution.

2. X-ray diffraction technique

The use of X-ray methods in the field of materials analysis is now entering its eighth decade. X-ray diffraction techniques are a very useful characterization tool to study, non-destructively, the crystallographic structure, chemical composition and physical properties of materials and thin films. It can also be used to measure various structural properties of these crystalline phases such as strain, grain size, phase composition, and defect structure.

2.1 X-rays creation

The processes of X-rays creation are based on the energy loss of the energetic electrons. **Figure 2a** shows the process of elastic and inelastic scattering where the deflection, or more specifically the acceleration during the deflection would always produce radiation.

Two routes including energy transfer between the incident electron and the electrons of the atom, exists. Both of these processes involve a primary ionization where a core electron is ejected from the atom. The ejected electron falls with an excess energy, which can be disposed as an X-ray or Auger electron [1]. The characteristic X-ray carries the full energy difference of the two electron states as shown in **Figure 2b**. Furthermore, an X-ray for a diffraction experiment is characterized by its wavelength, λ , but the energy, E , is typically more useful.

For XRD analysis, it is always required to use a coherent beam of monochromatic X-rays with a known wavelength [2]. That is why a right selection of metal anode and energy (i.e., a known wavelength) of accelerated electrons is very necessary.

2.2 Principle of measurements of X-rays diffraction

A crystal lattice consists of a regular arrangement of atoms, with layers of high atomic density existing throughout the crystal structure. Knowledge of how atoms are arranged into crystal structures and microstructures is the foundation on which we build our understanding of the synthesis, structure and properties of materials [1].

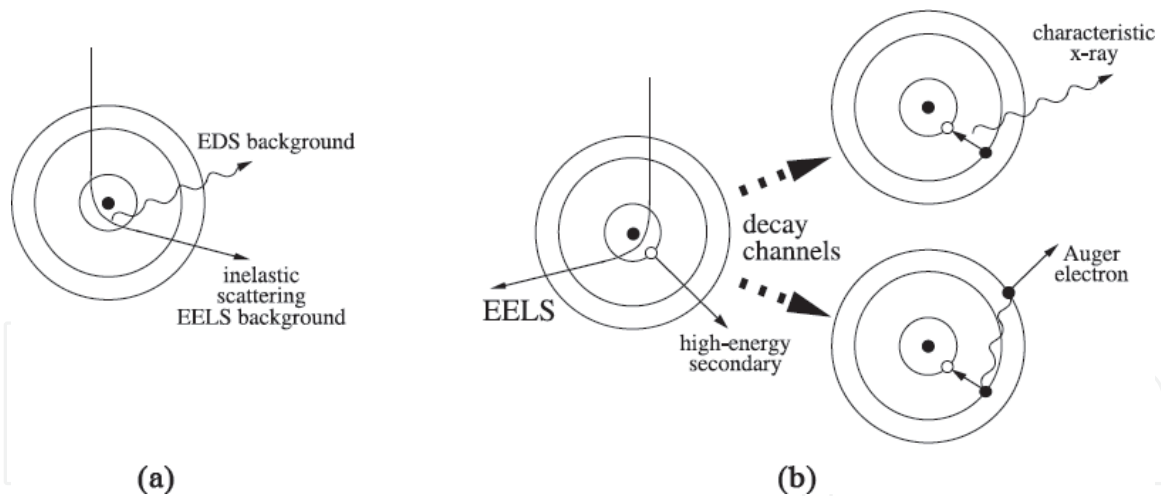


Figure 2.
 Interaction processes between a high-energy electron and an atom.

Planes of high atomic density means planes of high electron density. W.L. Bragg derived a simple equation treating diffraction as reflection from planes in the lattice.

$$n\lambda = 2d_{hkl} \sin\theta \quad (1)$$

where n is an integer, d_{hkl} is the distance inter reticular separating the plans defined by the indices from Miller (h, k, l), θ the angle of incidence and thus of reflexion compared to these plans and finally λ is the wavelength of photons X.

In fact, d_{hkl} does not represent the inter-reticular distance only, but it is defined too:

- the vector drawn from the origin of the unit cell to intersect the crystallographic plane (hkl) at a 90° angle, called also the vector magnitude;
- and, it is a geometric function of the size and shape of the unit cell.

Bragg's Law express and interpret the interaction of X-rays with sample, which creates secondary "diffracted" beams generated in the form of cones of X-rays. These beams are related to interplanar spacings in the crystalline powder according to the Bragg's mathematical relation.

Consequently, a family of planes produces a diffraction peak only at a specific angle 2θ . Diffraction experiments are generally made at a fixed wavelength (as we have mentioned above), thus a measure of the diffraction angles will allow the associated d-spacings to be calculated.

Figure 3 show the Bragg X-ray diffraction condition.

X-ray diffraction peaks are produced by constructive interference of monochromatic beam scattered from each set of lattice planes at specific angles. X-ray diffraction from crystalline solids occurs as a result of the interaction of X-rays with the electron charge distribution in the crystal lattice. The ordered nature of the electron charge distribution, which is distributed around atomic nuclei and is regularly arranged with translational periodicity, means that superposition of the scattered X-ray amplitudes will give rise to regions of constructive and destructive interference producing a diffraction pattern.

Bragg's equation tells us about the position of the diffraction peaks (in terms of θ), but tells us nothing about the intensity. The intensities of the diffraction peaks are determined by the arrangement of atoms in the entire crystal. These intensities can

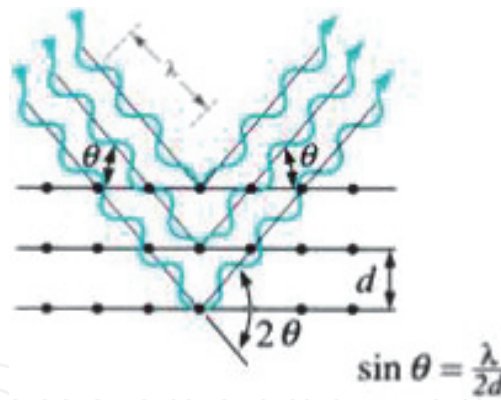


Figure 3.
Bragg X-ray diffraction condition [3].

be explained by the variation of the square of the structure factor according to the following equation [4]:

$$I_{hkl} \propto |F_{hkl}|^2 / F_{hkl} = \sum_{j=1}^M N_j f_j \exp \left[2\pi i (hx_j + ky_j + lz_j) \right] \quad (2)$$

This factor, F_{hkl} , represent the sums of resulting scattering from all of the atoms in the unit cell to form a diffraction peak from the (hkl) planes of atoms.

N_j is the fraction of every equivalent position that is occupied by atom j .

The three factors: x_j , y_j and z_j , which are the fractional coordinates, represents the atoms position in the atomic planes, and gives the first information about the amplitude of scattered light.

The other information of the amplitude of scattered light is given by the scattering factor f_j , which quantifies the efficiency of X-ray scattering at any angle by the group of electrons in each atom.

2.3 Sample preparation and diffractometer

Sample preparation is usually the most critical factor influencing the quality of the analytical data. Preferably, the sample should exhibit a plane or flattened surface.

All conventional X-ray spectrometers comprise three basic parts: the primary source unit, the spectrometer itself and the measuring electronics. The acquisitions are generally carried out using a goniometer θ - 2θ and by using a linear detector.

The diffraction pattern is collected by varying the incidence angle of the incoming X-ray beam by θ and the scattering angle by 2θ while measuring the scattered intensity $I(2\theta)$ as a function of the latter. Wide number of powder samples have been measured by using these tools, but it is also applied to the investigation of thin films.

Nowadays, CCD detector or scintillation are used in the novel generation of X-ray Diffractometer detector to record the angles and intensities of the diffracted beams with high resolution.

2.4 X-ray diffraction applications

X-ray Diffraction is considered as one of the most useful characterization techniques, because it is capable of providing general purpose qualitative and quantitative information on the presence of phases in an unknown mixture. This technique uses X-ray (or neutron) diffraction on powder or microcrystalline samples, where ideally every possible crystalline orientation is represented equally.

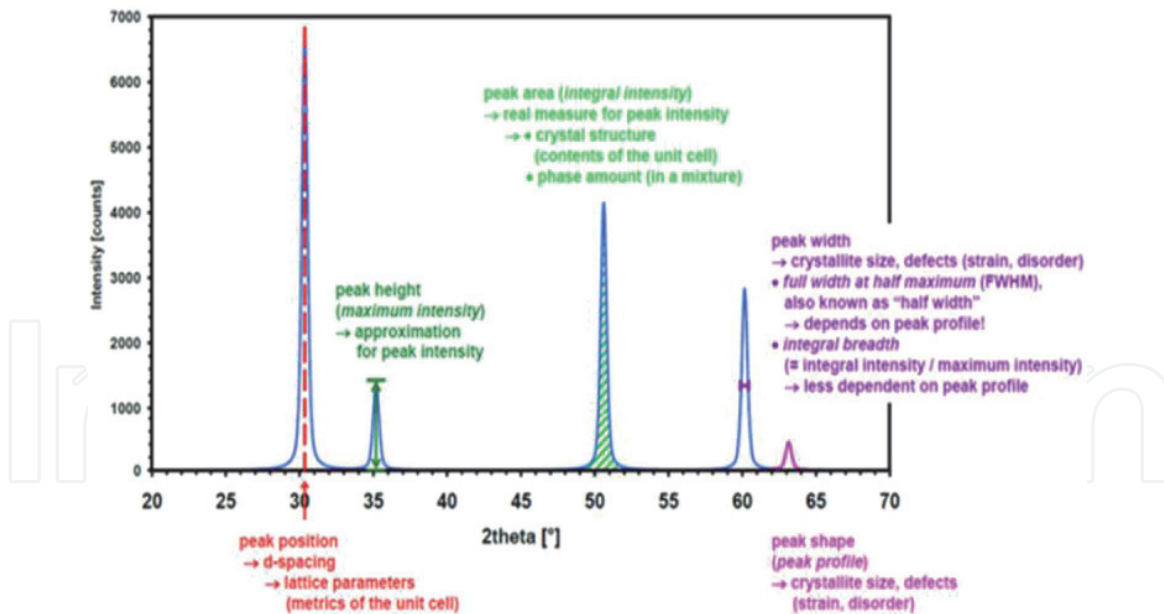


Figure 4.
 Information content of an idealized diffraction pattern [5].

Figure 4 shows the information we can get from an idealized diffraction pattern. A diffraction pattern contains a good deal of information of which three parameters are of special interest:

- The position of the diffraction maxima;
- The peak intensities;
- The intensity distribution as a function of diffraction angle.

The three pieces of information can be used in particular to identify and quantify the contents of the sample, as well as to calculate the material's crystallite size and distribution, crystallinity, stress and strain.

The most traditional use of XRD can be summarized as shown below.

Identification	<ul style="list-style-type: none"> • Phase identification (search/match): <ul style="list-style-type: none"> - In general by using the diffraction Patterns of Joint Committee on Powder Diffraction Standards (JCPDS); - The interreticular distances 'd' of the plans (hkl). • Determinations of unit cell parameters. • Grains size: <ul style="list-style-type: none"> - using the well known Sherrer formula.
Residual stress	<ul style="list-style-type: none"> • The principals of stress analysis by the X-ray diffraction is based on measuring angular lattice strain distributions.
Texture analysis	<ul style="list-style-type: none"> • Determination of the preferred orientation of the crystallites, usually described in terms of polefigures.

The diffraction pattern is like a fingerprint of the crystal structure. It is a powerful and rapid technique for identification of an unknown material.

2.4.1 Phases identification

Among these applications, the identification of unknown crystals in a sample seems to be the most important. The idea is to match the positions and the intensities of the peaks in the observed diffraction pattern to a known pattern of peaks from a standard sample or from a calculation.

A single crystal specimen in a diffractometer would produce only one family of peaks in the diffraction pattern as given in **Figure 5**. According to this figure, we can resume the most common cases of diffraction peaks identification used in reality.

From **Figure 5**, we can distinguish three cases:

- The first case for **Figure 5a** shows at $2\theta = 20.6^\circ$, that Bragg's law fulfilled for the (100) planes, producing a diffraction peak;
- The second for **Figure 5b**, the (110) planes would diffract at $2\theta = 29.3^\circ$; however, they are not properly aligned to produce a diffraction peak (the perpendicular to those planes does not bisect the incident and diffracted beams). Only background is observed;
- And the last one for **Figure 5c**, demonstrate that the (200) planes are parallel to the (100) planes. Therefore, they also diffract for this crystal. Since d_{200} is $\frac{1}{2} d_{100}$, they appear at $2\theta = 42^\circ$.

Nevertheless, a polycrystalline sample should contain thousands of crystallites as given in **Figure 5d**. Therefore, all possible diffraction peaks should be observed. For every set of planes, there will be a small percentage of crystallites that are properly oriented to diffract (the plane perpendicular bisects the incident and diffracted beams).

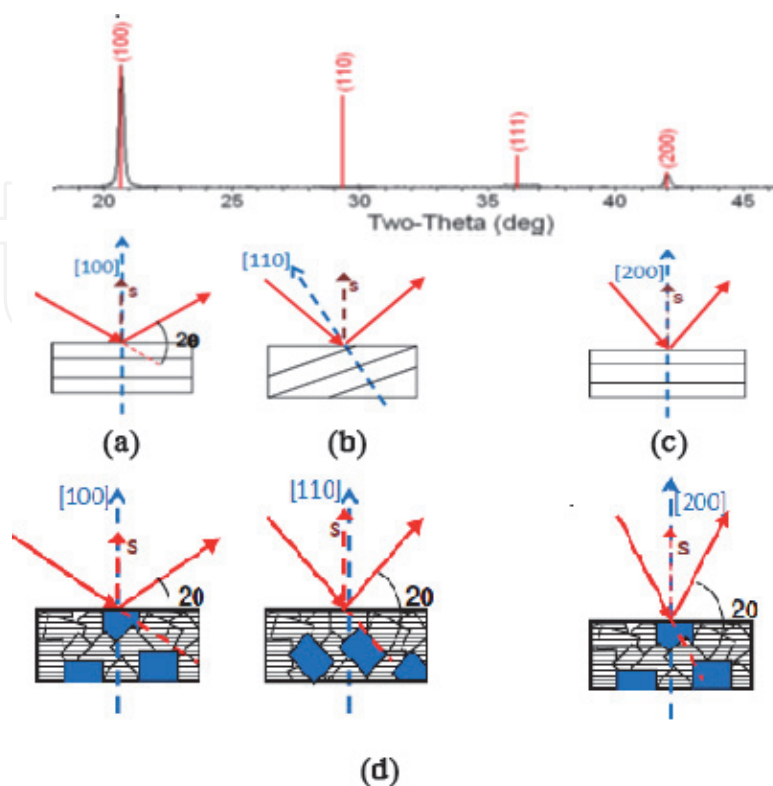


Figure 5.
Information content of an idealized diffraction pattern [5].

In addition, the position and the form of the peaks could give us some important information about the lattice stresses.

As shown in **Figure 6**, it can be clearly noticed the difference between the stressed and none stressed peaks. Cause, in the case of a uniform strain we note a peak move with no shape changes, contrary to the non-uniform strain which produce with the peak displacement a peak broadens.

2.4.2 Grain size

The determination of the crystallite size is based on the calculation of the width with middle height of peak (Full Width at Half Maximum FWHM) expressed in radian, according as mentioned before, to the well-known Sherrer formula (**Figure 7**).

The identification of this parameter is as follow:

An increase in the width of the diffraction causes a decrease in the crystallite size. Destructive interference of the all diffracted beams will result a sharp peak. Complete destructive interference beside the Bragg angle is produced from taking diffraction of large number of planes. Thereby, broadened peak can be observed when the crystallites are of very small sizes in which there are not enough planes to produce complete destructive interference.

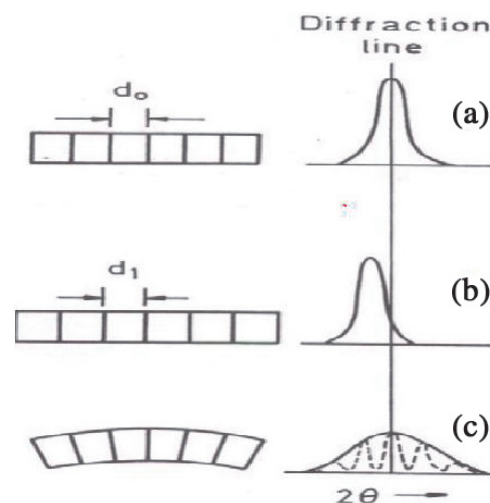


Figure 6.
 Strain effect on the diffraction peak [6].

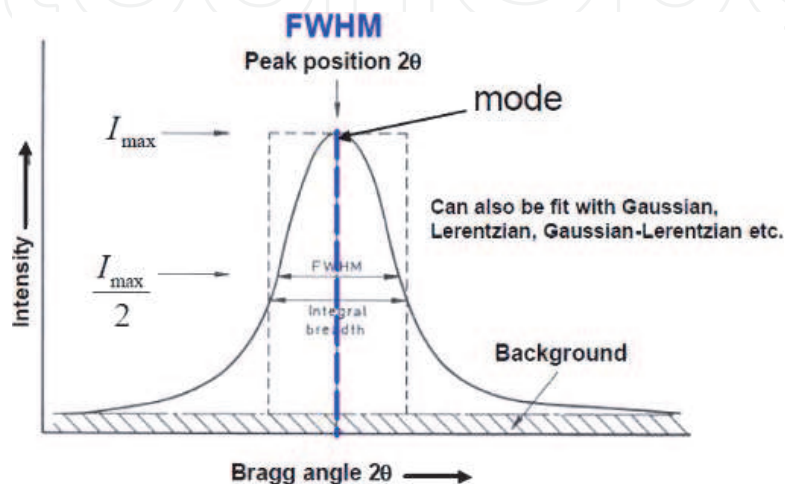


Figure 7.
 Determination of the FWHM [6].

3. Scanning electron microscopy

Since its first commercialization, Scanning Electron Microscope (SEM) shows a remarkable progress. This technique is now well known and used in many laboratories. A SEM can be utilized for high magnification imaging of almost all materials.

3.1 Principle

The SEM instrument is very suitable for different kinds of investigations. It is possible to investigate for example the fiber in wood and paper, metal fracture surfaces, production defects in rubber and plastic ect. [7]. Therefore, to be able to interpret the different images and information's collected by using SEM it is essential to understand the principal of function of this tool.

The principle of operation is as follows:

- In a vacuum enclosure, an electron beam focused sweeps the surface of the sample. According to the physicochemical nature of surface, secondary electrons, retrodiffused or Auger electrons are emitted, certain electrons are transmitted and others still dennent place has cathode-luminescence and x-rays as shown in **Figure 8**.
- According to the type of detector used, the retro diffused electrons provide an image topographic (contrast function of the relief) or an image of composition (contrast function atomic number).

For the observation of the PZT, a light metallization is necessary so to evacuate the loads.

3.2 Description of the microscope

A knowledgeable SEM operator should have a basic of contents, which can simplify at this point:

- A source (electron gun) of the electron beam which is accelerated down the column;
- A series of lenses (condenser and objective) which act to control the diameter of the beam as well as to focus the beam on the specimen;

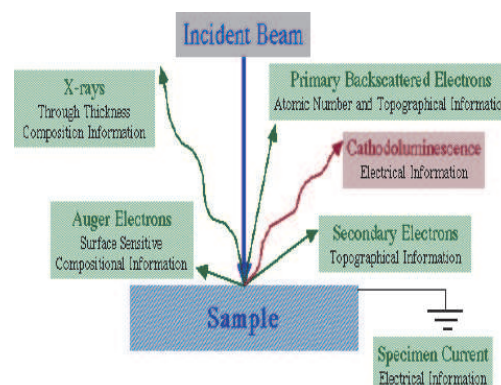


Figure 8.
Principle of electron beam/specimen interactions.

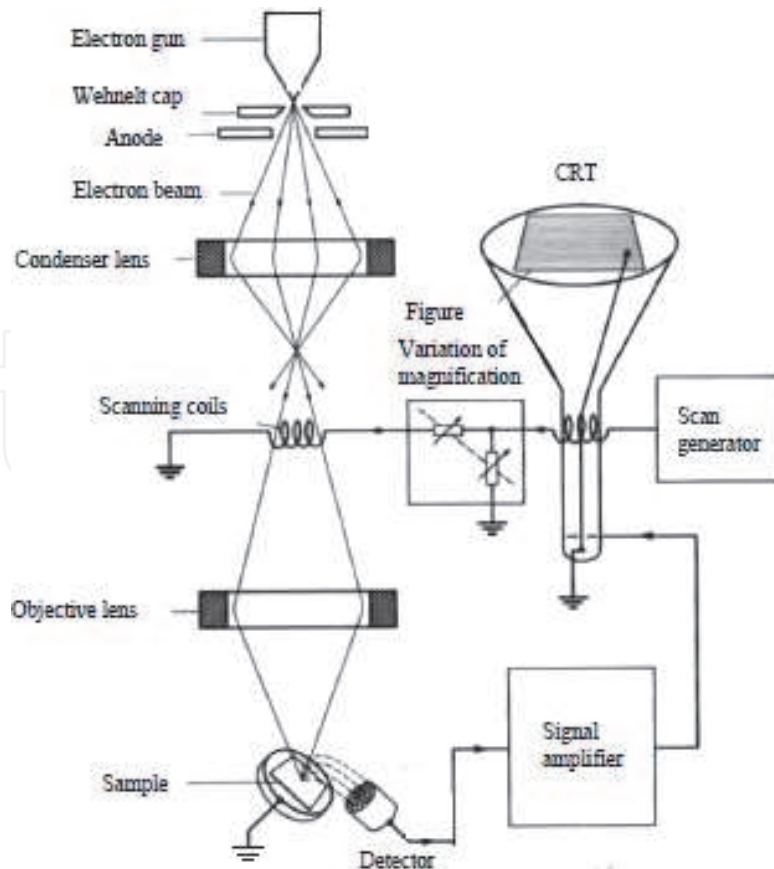
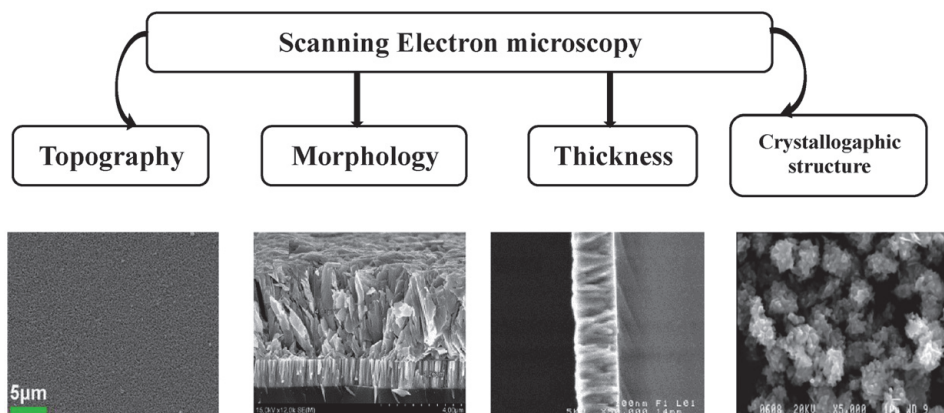


Figure 9.
 Scheme of scanning electron microscope [8].

- A series of apertures (micron-scale holes in metal film) which the beam passes through and which affect properties of that beam;
- Controls for specimen position (x, y, z-height) and orientation (tilt, rotation);
- An area of beam/specimen interaction that generates several types of signals that can be detected and processed to produce an image or spectra;
- System of pumping: 3 ionic pumps (vacuum of the column), a diffusion pump equipped with a vane pump (vacuum of the room) and a vane pump for hopper (**Figure 9**).

3.3 SEM applications

The different applications of this technique can be summarized as follow:



4. Energy dispersive spectroscopy EDS

Energy dispersive X-ray spectroscopy (EDS, EDX or EDXRF) is an analytical technique used for the elemental analysis or chemical characterization of a sample (Figure 10).

4.1 Principle

The operating principle of EDS is based on the interaction between electromagnetic radiation and matter; the X-rays emitted by the matter in response will be collected and analyzed. This analysis is due to the fact that each element has its own specific atomic structure; this latter allows the characteristic X-rays of the element atomic structure to be identified uniquely from each other (Figure 11) [9].

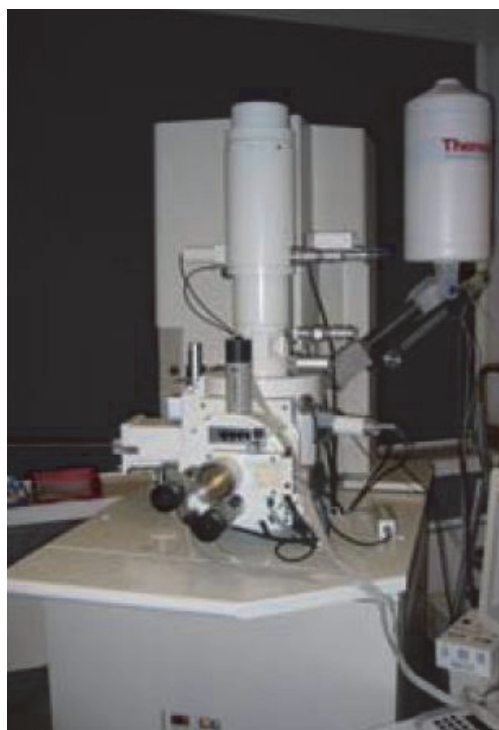


Figure 10.
Energy dispersive spectroscopy (EDS).

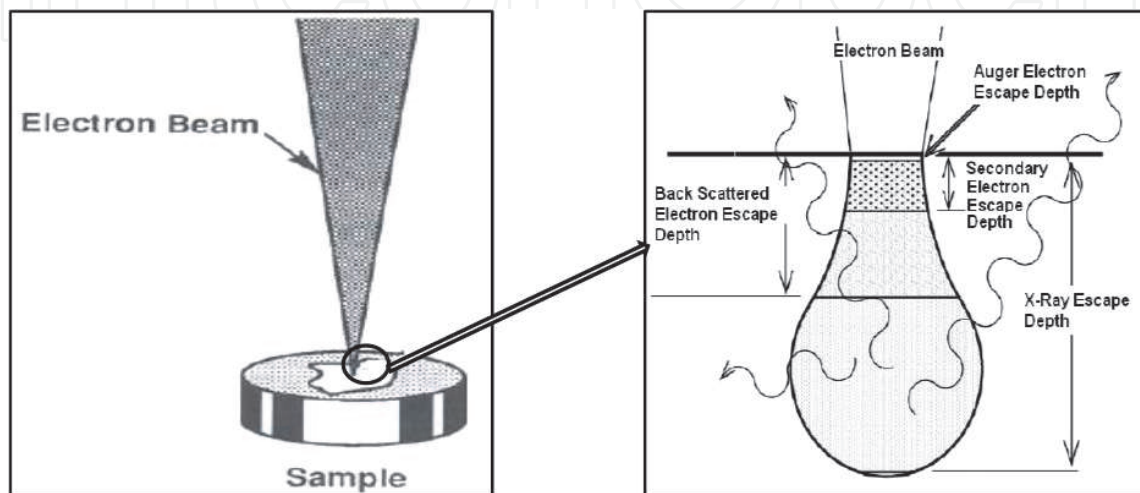


Figure 11.
X-ray source region, with path of X-rays to the spectrometer.

High energy beam of charged particles is focused into the sample being studied in order to stimulate the emission of characteristic X-rays from the specimen. Furthermore, an Energy Dispersive Spectrometer, EDS, is used in order to measure the number and energy of the X-rays emitted from a specimen. As the energy of the X-rays are characteristic of the difference in energy between the two shells, and of the atomic structure of the element from which they were emitted, this allows the elemental composition of the specimen to be measured [9].

4.2 EDS applications

The Energy-dispersive spectrometer is especially useful for qualitative analysis because a complete spectrum can be obtained very quickly, but is also used for the Quantitative analysis. This method permit to find what elements are present and their quantities in an 'unknown' specimen by identifying the lines in the X-ray spectrum using tables of energies or wavelengths (**Figure 12**) [10].

Six types of major artifacts may possibly be generated during the detecting process:

- Peak Broadening;
- Peak distortion;
- Silicon x-ray escape peaks;
- Sum peaks;
- Silicon and gold absorption edges;
- Silicon internal fluorescence peak.

5. Spectrophotometry

The spectrophotometer has well been called the workhorse of the modern laboratory. In particular, ultraviolet and visible spectrophotometry is the method of choice in most laboratories concerned with the identification and measurement of organic and inorganic compounds in a wide range of products and processes.

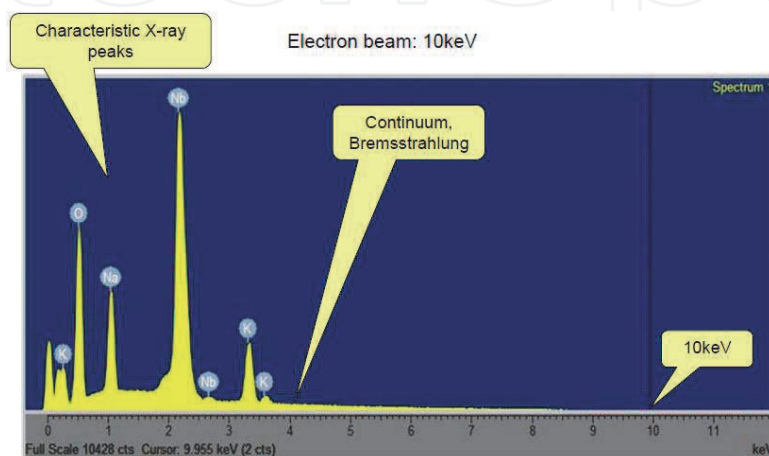


Figure 12.
EDX spectrum of $(K,Na)NbO_3$.

5.1 Principle

Spectrophotometry is commonly divided in two spectroscopic analyses:

- IR spectroscopy (Infrared spectroscopy), deals with the infrared region of the electromagnetic spectrum, that is light with a longer wavelength and lower frequency than visible light. It covers a range of techniques, mostly based on absorption spectroscopy. As with all spectroscopic techniques, it can be used to identify and study chemicals. The infrared spectrum of a sample is recorded by passing a beam of infrared light through the sample. When the frequency of the IR is the same as the vibrational frequency of a bond, absorption occurs.
- Ultraviolet–visible spectroscopy or ultraviolet–visible spectrophotometry (UV–Vis or UV/Vis) refers to absorption spectroscopy or reflectance spectroscopy in the ultraviolet–visible spectral region. This means it uses light in the visible and adjacent (near-UV and near-infrared (NIR)) ranges (Figure 13).

5.2 Description of the spectrophotometer

The instrument used in ultraviolet–visible spectroscopy is called a UV/Vis spectrophotometer (Figure 14).

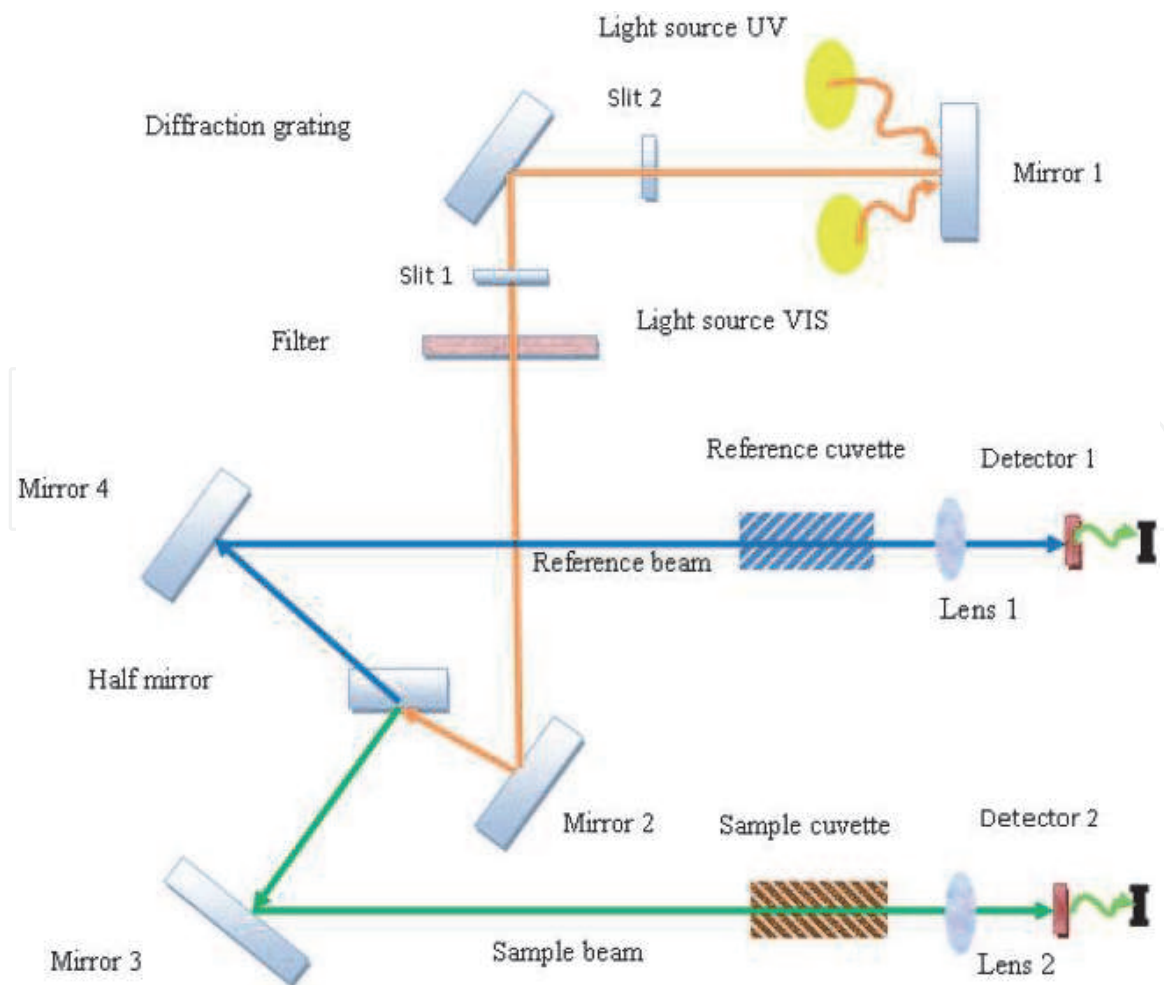


Figure 13.
Principle of operation UV–VIS spectrophotometer [11].

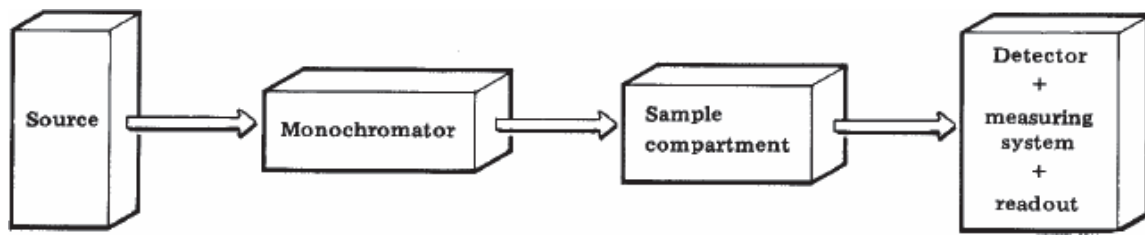


Figure 14.
Schematic drawing of spectrophotometer basic construction [12].

The minimum requirements of an instrument to study absorption spectra (a spectrophotometer) can be listed as below:

1. Radiation source with appropriate wavelengths.
2. Means of isolating light of a single wavelength and getting it to the sample compartment - monochromator and optical geometry.
3. Means of introducing the test sample into the light beam - sample handling.
4. Means of detecting and measuring the light intensity.

5.3 Spectrophotometer applications

Samples characterization by using UV/Vis spectrophotometry works by comparing the intensity light called reference (which represent the intensity of light before it passes through a sample), with the measured intensity of light passing through the sample. The ratio is called the transmittance (or absorbance), and is usually expressed as a percentage. Therefore by using a spectrometer we can measure Transmittance/Absorbance, and extract from it the following optical properties:

- Transmittance/Absorption;
- Energy gap;
- Activation energy;
- Disorder;
- Refraction index.

6. Hall Effect

Hall Effect is a process in which a transverse electric field is developed in a solid material when the material carrying an electric current is placed in a magnetic field that is perpendicular to the current. Hall Effect was discovered by Edwin Herbert Hall in 1879.

Hall effect is used to determine if a substance is a semiconductor or an insulator. The nature of the charge carriers, resistivity and carrier's mobility can be measured.

6.1 Principle and theory of Hall effect

The principle of Hall Effect states that when a current-carrying conductor or a semiconductor is introduced to a perpendicular magnetic field, a voltage can be

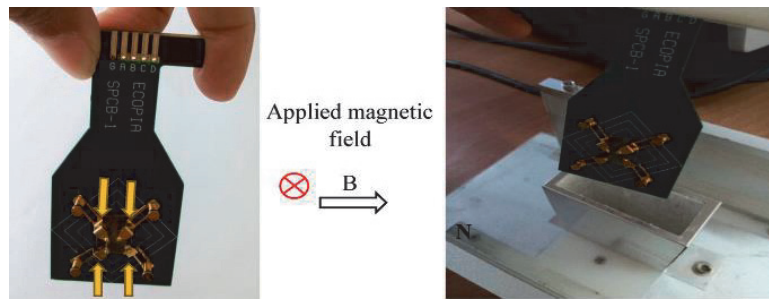


Figure 15. Hall measurement HMS set up of CuO grown onto glass substrate [13].

measured at the right angle to the current path. This effect of obtaining a measurable voltage is known as the Hall Effect (**Figure 15**).

When a conductive plate is connected to a circuit with a battery, then a current starts flowing. The charge carriers will follow a linear path from one end of the plate to the other end. The motion of charge carriers results in the production of magnetic fields. When a magnet is placed near the plate, the magnetic field of the charge carriers is distorted. This upsets the straight flow of the charge carriers. The force which upsets the direction of flow of charge carriers is known as Lorentz force.

Due to the distortion in the magnetic field of the charge carriers, the negatively charged electrons will be deflected to one side of the plate and positively charged holes to the other side. A potential difference, known as the Hall voltage will be generated between both sides of the plate which can be measured using a meter.

The Hall voltage represented as V_H is given by the formula:

$$V_H = (IB)/(qnd) \quad (3)$$

Here,

I: is the current flowing through the sensor;

B: is the magnetic Field Strength;

q: is the charge;

n: is the number of charge carriers per unit volume;

d: is the thickness of the sensor.

6.2 Hall coefficient

The Hall Coefficient R_H is mathematically expressed as.

$$R_H = E_y/(JB) \quad (4)$$

where: J is the current density of the carrier electron, E_y is the induced electric field and B is the magnetic strength. The hall coefficient is positive if the number of positive charges is more than the negative charges. Similarly, it is negative when electrons are more than holes.

7. Binary semiconductors layers' characterization

7.1 Tin monosulfide SnS

Tin monosulfide, SnS, seems to be one of the most important and the most studied binary semiconductor compounds [14]. Indeed, it can be used in many

technological devices [15]. It is specifically used in solar cells [15], as an absorber [16]. Stannous sulfide (SnS), is a very important candidate in photovoltaic application due to his high characteristics such as: direct band gap with an almost optimum value varying in the range 1.3–1.7 eV [17], high absorption coefficient ($\approx 10^5 \text{ cm}^{-1}$) [18] and the orthorhombic structure [15]. In addition, it has an orthorhombic structure [15].

By using a chemical ultrasonic spray deposition method (CUS) [13, 19–21], we have elaborated two samples of SnS thin films on glass substrates. Solution of (0.07 M) molarity was prepared by mixing tin chloride SnCl_2 and thiourea ($\text{SC}(\text{NH}_2)_2$) as sources of Sn and S respectively. The precursors were dissolved in methanol. The experimental details are given in **Table 1**.

X-ray diffraction patterns of deposited SnS thin films at different deposition time are shown in **Figure 16**.

The films were found to be polycrystalline with a relatively strong (120) peak. In addition, the other weak peaks contained in the diffraction pattern indicates that the prepared SnS films have the orthorhombic crystal structure according to the PDF Card No. 033–1375. Other additional peaks appearing at 28.73° , 32.72° and

Deposition time (min.)	Volume (ml)	Substrate temperature ($^\circ\text{C}$)	Nozzle–substrate distance (cm)
25	80	350	4.5
30			

Table 1.
 Experimental conditions used for the preparation of SnS thin films.

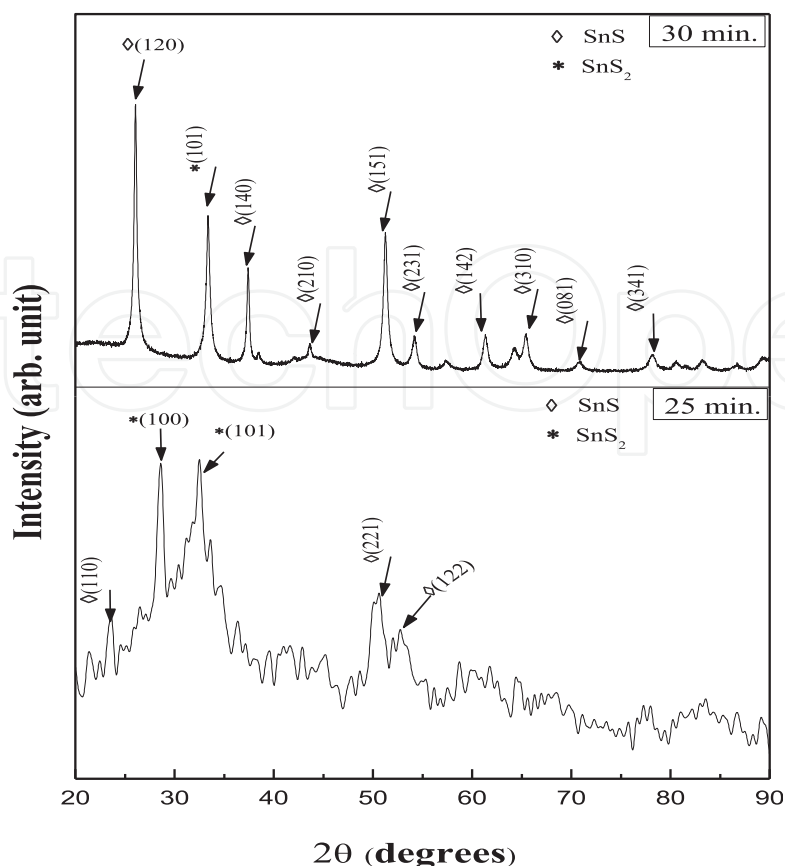


Figure 16.
 XRD patterns of SnS layers deposited at different deposition time [21].

49,78° can be attributed to the SnS₂ phase (PDF Card No. 031–1399) which was found to accompany the preparation of SnS [22].

The grain sizes and internal strains of the prepared films were calculated from the XRD data using the standard Debye–Scherer formula, and are summarized in **Table 2**.

The grain size calculated from the XRD diffraction spectrum varied from 16.54 nm to 19.07 nm when the deposition time was increased from 25 min. to 30 min. Similar values of the grain size have been found by other investigators [23, 24]. These sizes values indicate the nanocrystalline nature of the films.

Films morphology and chemical composition was carried out using scanning electron microscopy (SEM) and EDX technique. The typical SEM image of SnS thin film deposited during 30 min. is shown in **Figure 16**. The film is homogeneous, devoid of cracks and has a near stoichiometric ratio (Sn/S = 1.1). This smooth aspect of the obtained film (which is consistent with the XRD) can be related to the viscosity and the surface tension of methanol. Indeed, when using methanol as solvent, the droplets are more easily spread on the substrate surface [21]. Furthermore, we notice, the presence of Al, Cl, Si and O elements which are not expected to be in films and may originate from the glass substrates (**Figure 17**).

The optical band gap is calculated using the relation

$$(\alpha h\nu)^2 = A(h\nu - E_g) \quad (5)$$

where A is a constant, E_g is the optical band gap, ν is the frequency of the incident photon and h is the Planck's constant. The plots of $(\alpha h\nu)^2$ versus the photon energy $h\nu$ for direct transition for the film deposited during 30 min. is shown in **Figure 18**. The band gap energy of this film is determined using the intercept of the tangent to the plot with the abscissa axis.

The obtained optical band gap values of the two SnS thin films are summarized in **Table 3**. We notice that the optical band gap of the prepared films decreases when the deposition time increases. This decrease of the E_g can be due the grain size increase [25].

Deposition time (min.)	D (nm)	Internal strain ($\epsilon \times 10^{-3}$)
25	16,54	2,09
30	19,07	1,82

Table 2.
Grain sizes and internal strain of SnS films.

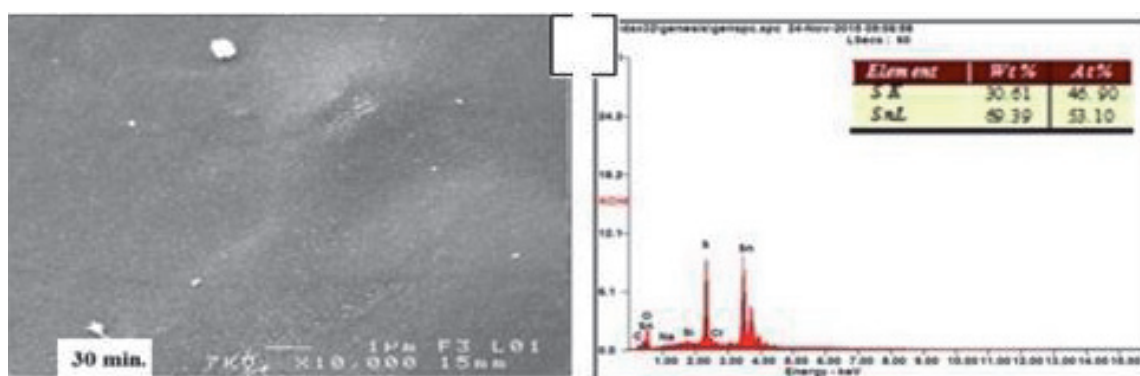


Figure 17.
SEM images and EDX spectrum of SnS film prepared during 30 min [21].

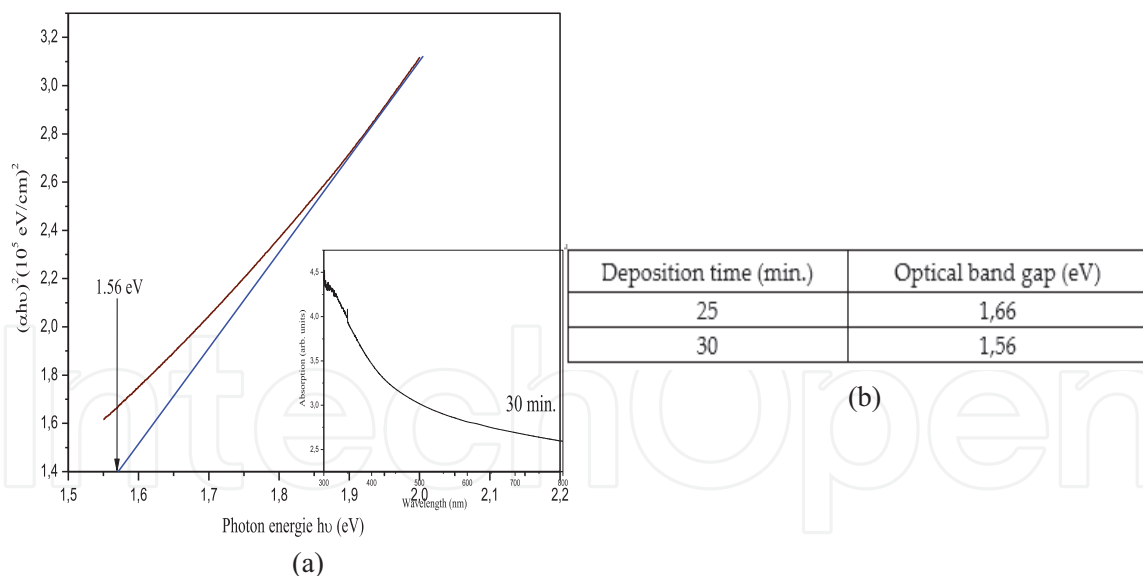


Figure 18. (A) Plot of $(\alpha h\nu)^2$ vs. $h\nu$ of SnS film. Inset: representation of the absorption coefficient α as a function of the wavelength. (B) Optical band gap of SnS films [21].

Deposition time (min.)	Sn / S (at.%)	Conduction type	Restivity ($\Omega\cdot\text{cm}$)
25	46.53 / 53.47	p-type	120
30	53.10 / 46.90	p-type	8.06

Table 3. Electrical conductivity of SnS films A and B and their deposition time.

In **Table 3** we report the electrical properties of the as-deposited SnS thin films. Stannous sulfide is generally known to be a p type semiconductor [26]. Ionized tin vacancies leads to create the acceptor levels [27].

The atomic ratio obtained from the EDX analysis, conduction type and resistivity are indicated in **Table 3**. We note that SnS films have an p-type conductivity, with quasi-stoichiometric composition. Since the conductivity type of the SnS films are essentially controlled by the excess in Sn concentration in the compound [21]. In this case, the Sn atoms act as donor and lead to the n-type conduction. But due to the quasi-stoichiometric nature of our films, they exhibit a p-type conductivity. Furthermore, we note that the resistivity of the films decreases when the deposition time increases. This variation can be attribute to the grain size increase as indicated in **Table 2**. These results are consistent with the literature [18].

7.2 Tin disulfide SnS₂

Tin disulfide (SnS₂) was considered as one of very interesting tin sulfides semi-conductors. SnS₂ has been known for its potential applications in solar cells as well as electrical switchings [28]. This material belongs to IV–VI group of semiconductor compound with hexagonal crystal structure ($a = 0.3648$ nm, $c = 0.5899$ nm) [29]. It has a wide band gap energy (2.88 eV) [30], and n-type electrical conductivity with magnitude depending on the preparation methods.

SnS₂ thin films were deposited onto ordinary glass substrates using the same method CUS as for SnS. The precursors used as sources of tin (Sn) and sulfur (S) are: (SnCl₄: 2H₂O) and (SC(NH₂)₂) respectively. Two different molarities of SnCl₄ (M_{Sn}) were diluted with a fixed molarity (0.1 mol/l) of thiourea (M_{S}) in methanol,

in order to study their effect on SnS₂ properties. These experimental conditions are summarized in **Table 4**.

Figure 19 shows the X-ray diffraction patterns of the elaborated films. From the obtained spectra it can be noticed, that the films are polycrystalline with a preferred orientation along the (001) direction and fit well with hexagonal SnS₂ structure according to the ASTM card number 23–0677. This indicates the presence of the pure hexagonal β-SnS₂ phase [31]. In addition, it can be noticed that, the main peak intensity increases with increasing M_{Sn} molarity.

Structural properties of the two samples are given in **Table 5**.

It can be noticed that the grain size decreases when the molarity increases, contrary to the strain. This comportment is due to the fact that grains growth is

Reagents molarity (mol/l)		Volume (ml)	Substrate temperature (°C)	Deposition time (min)
SnCl ₄ ·2H ₂ O	Thiourea			
0.06	0.1	30	350	10
0.07				

Table 4.

Experimental conditions used for tin disulfide thin films elaborations.

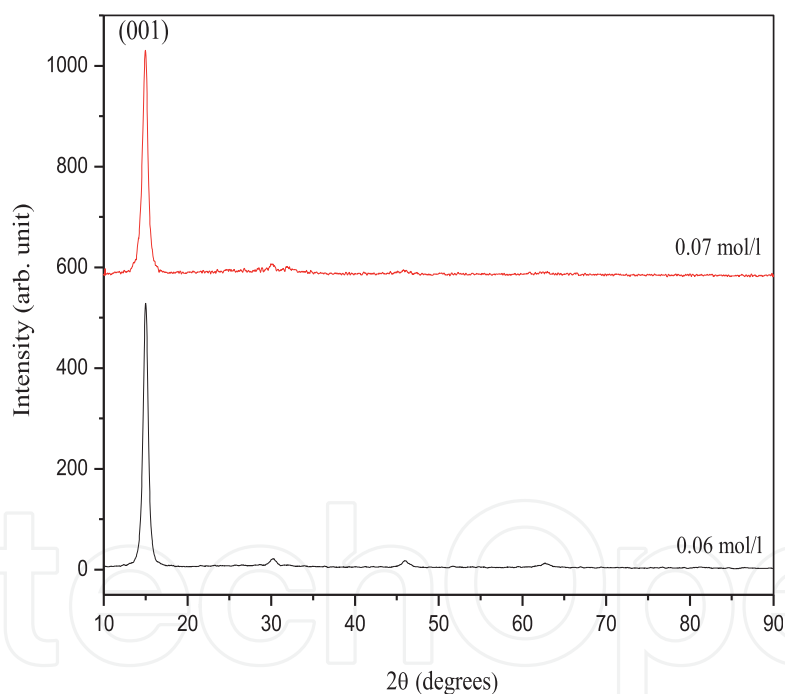


Figure 19.

XRD patterns of SnS₂ thin films deposited at different molarities [19].

Sample molarity (mol/l)	Cristallite size (nm)	Strain (*10 ⁻³) %	Lattice parameters (Å)	Lattice parameters (Å) according to JCPDS card number 23–0677
0.06	16.98	2,049	a = 3.613 c = 5.889	Hexagonal structure a = 3.648 c = 5.899
0.07	12.35	2,825	a = 3.603 c = 5.873	

Table 5.

Structural parameters of dominate phase of the prepared films.

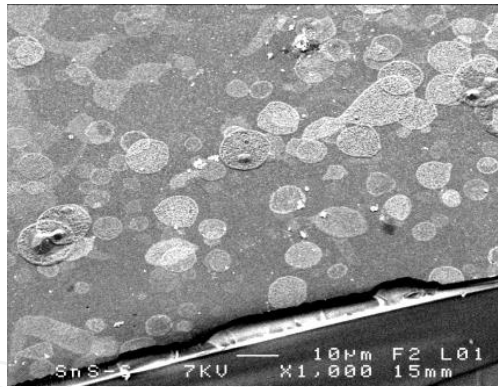


Figure 20.
SEM image of as-synthesized SnS₂ thin films [19].

controlled by the strain in film network. Because the presence of internal strain in the film network cause a minimization in the grain growth driving forces, which prevent the grain size enlargement during the film formation and vice-versa.

Morphological study of typical SnS₂ thin film ($M_{Sn} = 0.07$ mol/l), shows that the surface topography is dense and rough with an arbitrary distribution of the bubbles (**Figure 20**).

On the other hand, the measurement of films resistivity revealed that this latter decreases from $0.46 \times 10^3 \Omega \cdot \text{cm}$ when the molarity increases and reaches its minimum value of $0.18 \times 10^3 \Omega \cdot \text{cm}$ for $M_{Sn} = 0.07$ mol/l.


According to the obtained results, for the two studied materials, with the different analysis techniques we can conclude that the good quality of the deposited films and the low fabrication cost of the used method can lead to solar cells whose cost-quality ratio is better than the solar cells which are fabricated by the other standard process.

Author details

Kenza Kamli* and Zakaria Hadeif
Department of Physics, Faculty of Sciences, University 20 Août 1955-Skikda,
Skikda, Algeria

*Address all correspondence to: kenza_kamli@yahoo.fr; k.kamli@univ-skikda.dz

IntechOpen

© 2021 The Author(s). Licensee IntechOpen. This chapter is distributed under the terms of the Creative Commons Attribution License (<http://creativecommons.org/licenses/by/3.0>), which permits unrestricted use, distribution, and reproduction in any medium, provided the original work is properly cited. 

References

- [1] Transmission electron microscopy and diffractometry of materials “Chapter 1 Diffraction and the X-Ray Powder Diffractometer”. Fultz B., Howe J.M., 2013, XX, 764 p., Hardcover. ISBN: 978-3-642-29760-1
- [2] James R. Connolly, for EPS400–002, Introduction to X-Ray Powder Diffraction, Spring 2007
- [3] Serna F, Lagneau J, Carpentier JM. La diffraction des rayons X : une technique puissante pour résoudre certains problèmes industriels et technologiques. Chimie Nouvelle. 2014; 116.
- [4] M. Birkholz, Thin Film Analysis by X-Ray Scattering. Copyright c 2006 WILEY-VCH Verlag GmbH & Co. KGaA, Weinheim ISBN: 3-527-31052-5.
- [5] Sharma R, Bisen DP, Shukla U, Sharma BG. X-ray diffraction: a powerful method of characterizing nanomaterials. Recent Research in Science and Technology. 2012; 4(8): 77-79.
- [6] http://www.chem.ox.ac.uk/icl/heyas/structure_of_solids/Lecture1/Bravais.gif
- [7] Agarwal B.K. X-ray Spectroscopy, 2nd edn, Springer-verlag, Berlin, 1991.
- [8] Goldstein, J. I., et al. Scanning Electron Microscopy and X-ray Microanalysis, 3rd ed, Plenum Press, New York, 2003.
- [9] Cantoni M., Introduction to EDX, MSE-636 Spring, 2014.
- [10] Reimer L., Scanning Electron Microscopy, Springer-Verlag, Berlin, 1985.
- [11] Kamli K., Elaboration et caractérisations physico-chimique des couches minces de sulfure d'étain par spray ultrasonique: Effet des sources d'étain, Master thesis, Mohamed Khider-Biskra University, 2013.
- [12] Basic UV/Visible Spectrophotometry.
- [13] Kamli K., Hadeif Z., Chouial B., Hadjoudja B., Thickness effect on electrical properties of copper oxide thin films, Surface Engineering, <https://doi.org/10.1080/02670844.2018.1475052>, 2018.
- [14] A. Sánchez-Juárez, A. Tiburcio-Silver, A. Ortiz, ‘Fabrication of SnS₂/SnS heterojunction thin film diodes by plasma-enhanced chemical vapor deposition’, Thin Solid Films, 2005, 480–481, 452–456.
- [15] Sekhar C. Ray, Malay K. Karanjai, Dhruva DasGupta, ‘Structure and photoconductive properties of dip-deposited SnS and SnS₂ thin films and their conversion to tin dioxide by annealing in air’ Thin Solid Films, 1999, 350, 72-78.
- [16] M.M. El-Nahass, H.M. Zeyada, M.S. Aziz, N.A. El-Ghamaz, ‘Optical properties of thermally evaporated SnS thin films’, Opt. Mter. 2002, 20, 159-170.
- [17] Jacob A. Andrade-Arvizu, M.F. García-Sánchez, M. Courel-Piedrahita, J. Santoyo-Morales, D. Jiménez-Olarte, M. Albor-Aguilera, O. Vigil-Galán, ‘Pressure induced directional transformations on close spaced vapor transport deposited SnS thin films, Materials and Design, 2016, 110, 878–887.
- [18] E. Guneri, C. Ulutas, F. Kirmizigul, G. Altindemir, F. Gode, C. Gumus, ‘Effect of deposition time on structural, electrical, and optical properties of SnS thin films deposited by chemical bath deposition’, Applied Surface Science, 2010, 257, 1189–1195.

- [19] Hadeif Z., Kamli K., Attaf A., Aida M. S. and Chouial B., Effect of SnCl_2 and SnCl_4 precursors on SnS_x thin films prepared by ultrasonic spray pyrolysis, *Journal of Semiconductors*, 38 (2017) 6.
- [20] Kamli K., Hadeif Z., Chouial B., Hadjoudja B., Elaboration of SnS_2 Thin Films by Ultrasonic Spray for Solar Cell Application, *Global Journal of Researches in Engineering: J General Engineering*, 17 (2017) 5.
- [21] Kamli K., Hadeif Z., Chouial B., Hadjoudja B., Zaidi B., Chibani A., Synthesis and characterisation of tin sulphide thin films, DOI: 10.1080/02670844.2016.1271593, 2017.
- [22] Li Q., Ding Y., Wu H., Liu X., Qian Y., 'Fabrication of layered nanocrystallites SnS and $\beta\text{-SnS}_2$ via a mild solution route', *Mater. Res. Bull.*, 37 (2002) 925-932.
- [23] Sajeesh T.H., Jinesh K.B., Sudha Kartha C., Vijayakumar K.P., 'Role of pH of precursor solution in taming the material properties of spray pyrolysed SnS thin films', *Applied Surface Science*, 258 (2012) 6870–6875.
- [24] Panda S.K., Antonakos A., Liarokapis E., Bhattacharya S., Chaudhuri S., 'Optical properties of nanocrystalline SnS_2 thin films', *Materials Research Bulletin*, 42 (2007) 576–583.
- [25] Guneri E., Gode F., Ulutas C., Kirmizigul F., Altindemir G., Gumus C., 'Properties of p-type SnS thin films prepared by chemical bath deposition', *Chalcogenide Lett.*, 2010, 7, 685–694.
- [26] Guneri E, Gode F, Ulutas C, et al. Properties of p-type SnS thin films prepared by chemical bath deposition. *Chalcogenide Lett.* 2010;7:685–694.
- [27] Vidal J, Lany S, d'Avezac M, et al. Band-structure, optical properties, and defect physics of the photovoltaique semiconductor SnS . *Appl Phys Lett.* 2012;100:032104.
- [28] Bissessur R., Schipper D., Exfoliation and reconstruction of SnS_2 layers: A synthetic route for the preparation of polymer- SnS_2 nanomaterials, *Materials Letters* 62 (2008) 1638–1641.
- [29] Chakrabarti A., Lu J., McNamara A. M., Kuta L. M., Stanley S. M., Xiao Z., Maguire J. A., Hosmane N. S., Tin (IV) sulfide: Novel nanocrystalline morphologies, *Inorganica Chimica Acta* 374 (2011) 627–631.
- [30] Tan F., Qu S., Zeng X., Zhang C., Shi M., Wang Z., Jin L., Bi Y., Cao J., Wang Z., Hou Y., Teng F., Feng Z., Photovoltaique effect of tin disulfide with nanocrystalline/amorphous blended phases, *Solid State Communications* 150 (2010) 58–61.
- [31] Benouis C E, Benhaliliba M, Yakuphanoglu F, et al. Physical properties of ultrasonic sprayed nanosized indium doped SnO_2 films. *Synthetic Metals*, 161 (2011) 1509.